



Retinal Nerve Fiber Layer Optical Texture Analysis

Involvement of the Papillomacular Bundle and Papillofoveal Bundle in Early Glaucoma

Christopher K.S. Leung, MD, MBChB,^{1,2,3} Philip Yawen Guo, MSc,¹ Alexander K.N. Lam, PhD¹

Purpose: To apply retinal nerve fiber layer (RNFL) optical texture analysis (ROTA) in eyes with early glaucoma to investigate (1) the pattern of RNFL defects, (2) how often the papillomacular bundle and papillofoveal bundles are involved, and (3) the association between papillomacular and papillofoveal bundle defects and visual field (VF) sensitivity abnormalities.

Design: Cross-sectional study.

Participants: Two hundred four eyes with early glaucoma (VF mean deviation, ≥ -6 dB) with RNFL defects from 171 consecutively enrolled patients with glaucoma.

Methods: All eyes underwent 24-2 VF testing and OCT for ROTA. The borders of RNFL defects were delineated from ROTA, and the involvement of the arcuate bundle, papillomacular bundle (i.e., bundles from the macula, excluding the fovea), and papillofoveal bundle (i.e., bundles from the fovea) was determined for each eye. Multilevel logistic regression analysis was applied to evaluate the structure–function association.

Main Outcome Measures: Proportions of eyes with papillomacular or papillofoveal bundle defects.

Results: Of the 204 eyes, 71.6% and 17.2% demonstrated RNFL defects involving the papillomacular and papillofoveal bundles, respectively; 25.0% showed arcuate bundle defects without involvement of papillomacular or papillofoveal bundles. The pattern of RNFL defects was diverse; the most common was concomitant involvement of the inferior arcuate bundle and the inferior papillomacular bundle (20.6%). Papillomacular or papillofoveal bundle defects were not associated with VF defects (i.e., with ≥ 3 contiguous locations with abnormal VF sensitivity in the pattern deviation probability plot) in the corresponding hemifield, although VF sensitivity of any 1 of the central 4 VF locations of the 24-2 test, which were within the macula, was more likely to be abnormal ($P < 0.05$ in the pattern deviation probability plot; odds ratio, 12.5; 95% confidence interval, 7.0–22.5) when the VF stimulus was projected onto a papillomacular or papillofoveal bundle defect than that projected onto an intact papillomacular or papillofoveal bundle.

Conclusions: Contrary to the conventional notion that the fovea and macula are not affected until the late stages of glaucoma, papillofoveal and papillomacular bundle defects were common in early glaucoma, and they were associated with central VF sensitivity loss at the corresponding VF test locations. *Ophthalmology* 2022;■:1–13 © 2022 by the American Academy of Ophthalmology. This is an open access article under the CC BY license (<http://creativecommons.org/licenses/by/4.0/>).



Supplemental material available at www.aaojournal.org.

Although clinical examination of the retinal nerve fibers was first described by Vogt¹ in 1913 when he pioneered red-free illumination of the retina with direct ophthalmoscopy, it was not until 1973 that Hoyt et al² adapted Vogt's method and described slitlike retinal nerve fiber layer (RNFL) defects in glaucoma. Since then, red-free RNFL photography has become a standard technique to examine RNFL defects. Although RNFL defects are visualized best over the superior and inferior arcuate bundles, defects involving the papillomacular bundle and the papillofoveal bundle, that is, axonal fiber bundles emanated from the macula and fovea,

respectively, are hardly discernible with red-free photographs because the RNFL is thin and the scattering is weak at the macula (Fig 1, first column).

The introduction of time-domain OCT in 1991 allowed measurement of RNFL thickness over the circumpapillary region.³ With a higher scan speed and a higher scan density provided by the Fourier-domain OCT, measurement of RNFL thickness over a wide field, including the parapapillary region and the macula, has become feasible.^{4–6} Different from red-free RNFL photographs in which RNFL defects can be visualized from the loss of RNFL scattering, RNFL

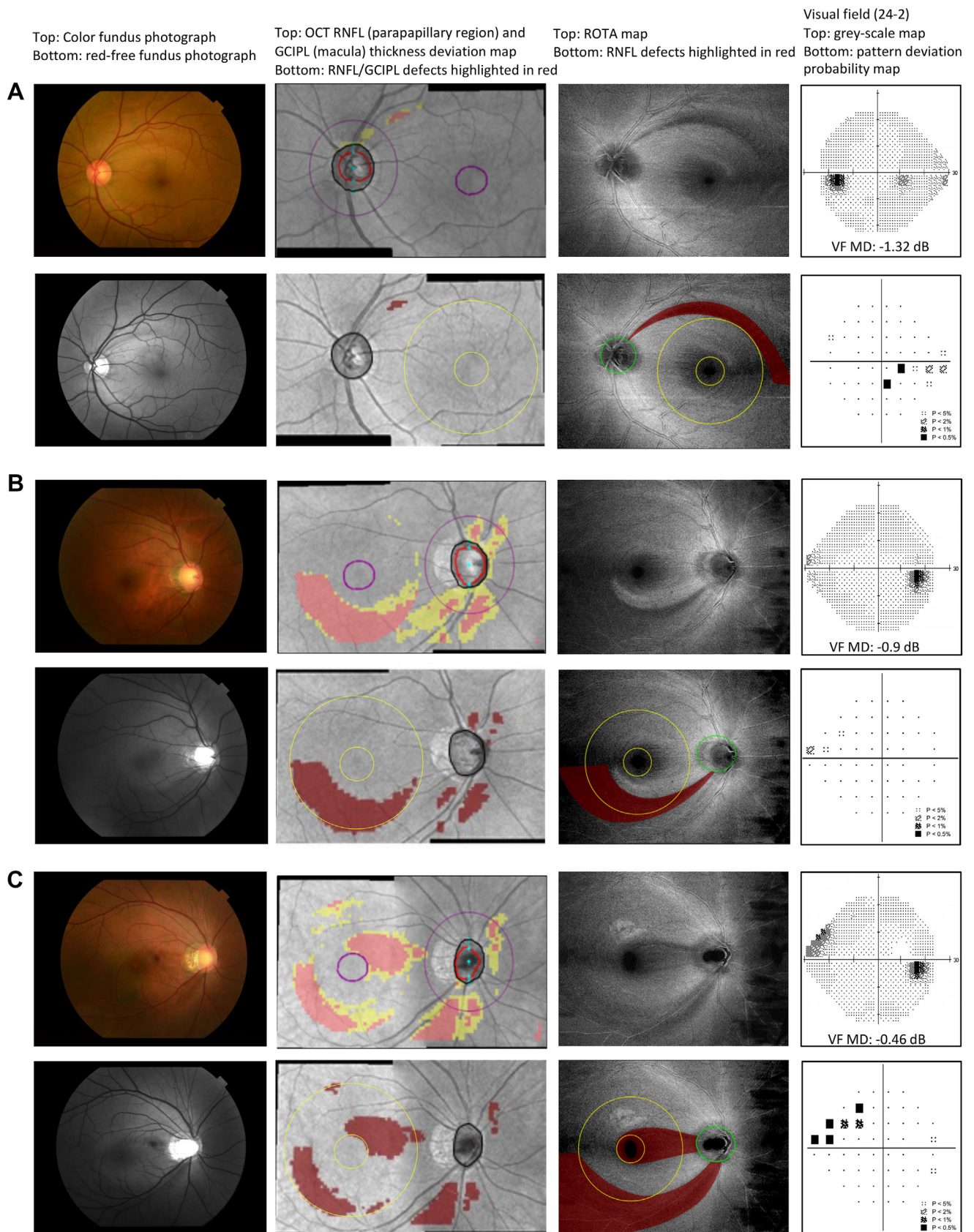


Figure 1. Comparison of retinal nerve fiber layer (RNFL) optical texture analysis (ROTA), color fundus photography, red-free RNFL photography, and OCT parapapillary RNFL and macular ganglion cell–inner plexiform layer (GCIPL) thickness analysis to discern the extent and the location of RNFL

defects in OCT conventionally are detected from the RNFL thickness probability or deviation map, with pixels encoded in red or yellow when the pixel RNFL thickness is less than the first or the fifth percentiles, respectively. However, determining the location and the extent of RNFL defects with the RNFL thickness probability or deviation map is complicated by the fact that the borders of RNFL defects may not align with the trajectories of the axonal fiber bundles (Fig 1, second column). Retinal nerve fiber layer defects not conforming to the trajectories of the axonal fiber bundles may suggest false-positive findings, which are common in the diagnostic evaluation of glaucoma using OCT.^{7,8}

With increasing awareness of detecting functional and structural deficits over the macula in glaucoma,^{9–12} a reliable approach to examine RNFL defects over the papillomacular and papillofoveal bundles is vital. We recently devised RNFL optical texture analysis (ROTA), a new algorithm to uncover the trajectories of the axonal fiber bundles over a wide field via displaying the optical texture signatures of axonal fiber bundles embedded in OCT scans.¹³ In addition to the arcuate bundles, ROTA distinctively reveals the trajectories of papillomacular and papillofoveal bundles (Fig 1, third column; Fig S1, fourth column, available at www.aaojournal.org), which are difficult to recognize from red-free photographs because the visibility of the RNFL declines with age and in eyes with a hypopigmented fundus, media opacities, or diffuse RNFL thinning¹⁴ and is indiscernible from conventional OCT analysis. Being able to determine the location and the extent of RNFL defects within and beyond the macula in precision, it is feasible to map individual visual field (VF) stimulus projections topographically onto the ROTA map to unfold the location-by-location structure–function association (Fig 2). Applying ROTA in 204 eyes with early glaucoma from 171 patients recruited consecutively in this study, we asked what the most common patterns of RNFL defects in early glaucoma were, how often the papillomacular and papillofoveal bundles were involved, and how likely a VF stimulus projected onto a papillomacular or papillofoveal bundle defect shows an abnormal sensitivity.

Methods

Patients

We selected eyes with early glaucoma (i.e., VF mean deviation [MD], ≥ -6 dB) and RNFL defects in ROTA from a pool of 448 patients with glaucoma who were recruited consecutively from Hong Kong Eye Hospital, Chinese University of Hong Kong Eye Clinic, and Prince of Wales Hospital between August 2015 and October 2018 at the screening visit of 3 clinical studies.^{15–17} These

patients were followed up at the University of Hong Kong Glaucoma and Optic Nerve Diagnostic Center. Among the 685 eyes (448 patients) with clinical evidence of glaucoma (i.e., a thinned RNFL and narrowed neuroretinal rim in at least 1 eye as determined by a glaucoma specialist during clinical examination, with or without VF defects),¹⁸ 475 eyes were excluded because of VF MD of < -6 dB (351 eyes), unreliable VF results (20 eyes), macular pathologic features (30 eyes), or suboptimal OCT scan quality (74 eyes). Six eyes with VF MD of -6 dB or more also were excluded because they showed no detectable RNFL defects in ROTA. Consequently, 204 eyes (171 patients) with VF MD of -6 dB or more and RNFL defects in ROTA were analyzed. Glaucoma was diagnosed when no history of neurologic disease was present to account for the rim, RNFL, VF abnormalities, or both. To be eligible for inclusion, the patient had to be 18 years of age or older with no history of macular disease or refractive or retinal surgery; the included eye had to have visual acuity of 20/40 or better and no evidence of pathologic features of myopia, such as lacquer cracks and chorioretinal atrophy.¹⁹ All participants underwent measurement of visual acuity, refraction, axial length (partial coherence laser interferometry), slit-lamp biomicroscopy of the anterior and posterior segments, Goldmann applanation tonometry, VF testing (Humphrey Field Analyzer II-i; Carl Zeiss Meditec), and widefield OCT imaging (Triton OCT; Topcon) for ROTA during the same visit. Both eyes of a patient were analyzed if both eyes were eligible for inclusion. The study adhered to the tenets of the Declaration of Helsinki and was approved by the Hong Kong Hospital Authority research ethics committees. Written informed consent was obtained from all participants.

Perimetry

All eyes underwent standard automated white-on-white perimetry using the 24-2 Swedish Interactive Threshold Algorithm Standard strategy in the Humphrey Field Analyzer II-i. We selected the 24-2 test instead of the 10-2 test because the latter would miss VF sensitivity abnormality associated with arcuate bundle defects (the superior and inferior arcuate bundles are located beyond the central 20°). Results of a VF test were considered reliable if fixation losses were 20% or less and false-positive errors were 15% or less. A VF defect had 3 or more significant ($P < 0.05$) nonedge contiguous points on the same side of the horizontal meridian with at least 1 with $P < 0.01$ in the pattern deviation probability plot and confirmed on at least 3 consecutive visits.²⁰

OCT RNFL Imaging and ROTA

All eyes underwent OCT RNFL imaging (Triton OCT; Topcon) over a wide field (12×9 mm²) covering the parapapillary region and the macula. OCT RNFL reflectance and RNFL thickness measurements of individual eyes were exported via a proprietary research browser provided by Topcon to a computer for ROTA. The algorithm of ROTA has been described.¹³ Whereas previous studies showed a reduction in the reflectance of RNFL as measured by OCT in eyes with glaucoma or ocular

defects in early glaucoma. **A**, Superotemporal RNFL defect can be visualized vaguely from the fundus and red-free photographs and can be detected as an isolated patch of RNFL thickness abnormalities in the OCT RNFL thickness analysis; ROTA unambiguously identifies a wedge-shaped superotemporal RNFL defect that corresponds to the inferonasal visual field (VF) defect. **B**, Inferotemporal RNFL defect can be detected in the fundus and red-free photographs, although the borders of the RNFL defect are indistinct. Islands of RNFL and GCIPL thickness abnormalities with distinct borders are found in the OCT RNFL and GCIPL thickness deviation map, but they do not conform to the trajectories of the axonal fiber bundles; ROTA reveals a wedge-shaped inferotemporal RNFL defect with borders following the trajectories of axonal fiber bundles. **C**, Inferotemporal RNFL defect is evident in the color fundus and red-free photographs, but it is unclear whether RNFL defects exist over the macula. Conventional OCT analysis shows multiple RNFL and GCIPL defects; ROTA uncovers 2 RNFL defects: an inferotemporal RNFL defect and a papillofoveal bundle defect. MD = mean deviation.

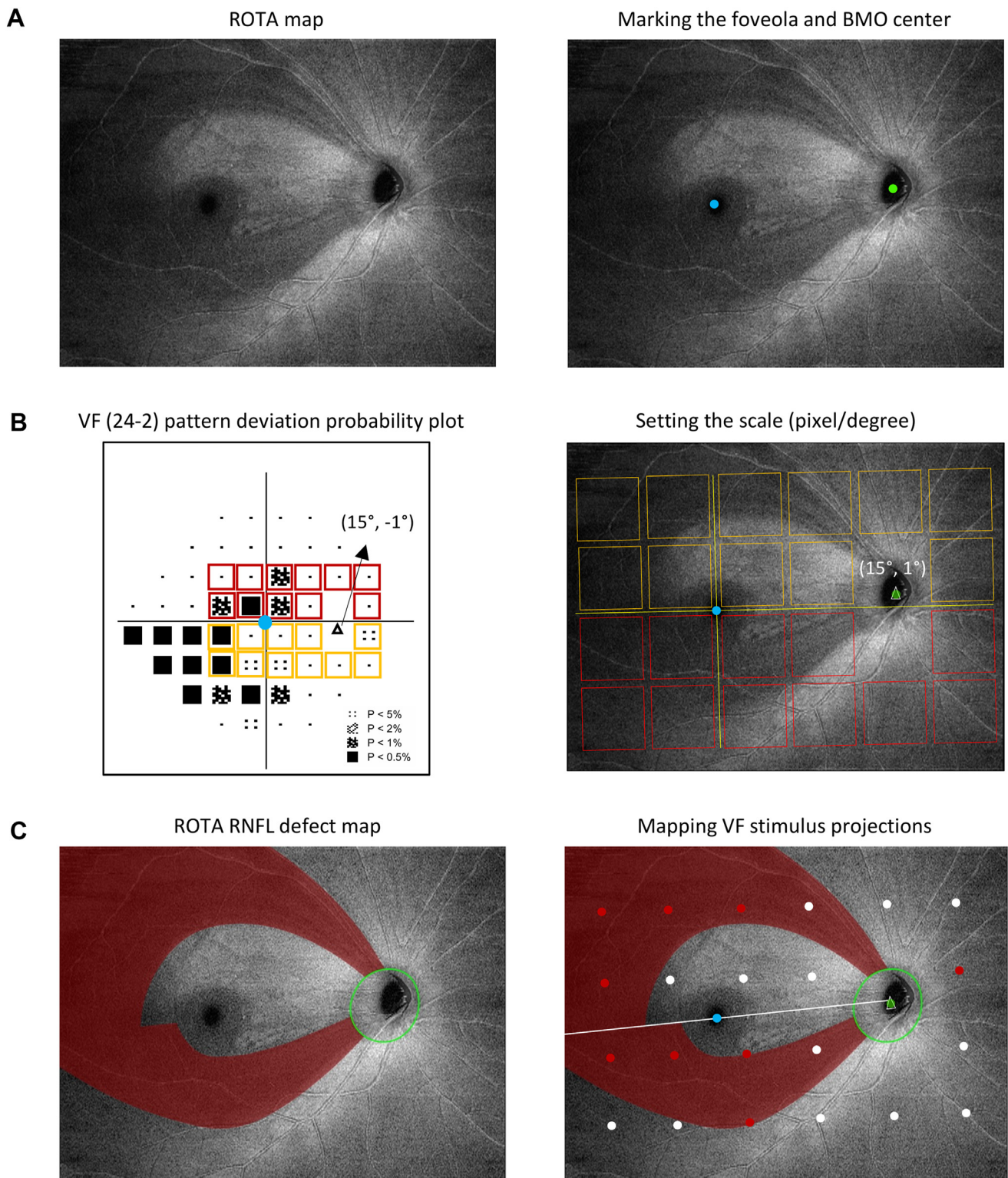


Figure 2. Mapping of visual field (VF) stimulus projections onto the retinal nerve fiber layer (RNFL) optical texture analysis (ROTA) map. **A**, Bruch's membrane opening (BMO) center (green dot) and the foveola (blue dot) were marked on the ROTA map as described in Methods. **B**, Coordinates of the center of blind spot (denoted by a triangle in the pattern deviation probability plot) ($15^{\circ}, -1^{\circ}$) relative to the central fixation ($0^{\circ}, 0^{\circ}$) (left panel) were exported from the VF analyzer and transposed onto the BMO center and foveola of the ROTA map, respectively, to set the scale (pixels per degree) for mapping of the VF stimulus projections onto the ROTA map (right panel). **C**, Individual VF stimulus projections, 0.43° in size (Goldmann size III) and spaced 6° apart, in the superior hemifield were mapped to the inferior hemiretina and vice versa. Red dots on the ROTA map represent locations with a VF pattern deviation probability value of $< 5\%$; white dots represent locations with a VF pattern deviation probability value of $> 5\%$.

hypertension,^{21,22} ROTA discerns specific patterns of RNFL defects over a wide field of the retina via uncovering the trajectorial details of axonal fiber bundles by integrating RNFL reflectance and RNFL thickness measurements with a series of nonlinear transformations.¹³ Retinal nerve fiber layer defects can be identified distinctively from ROTA because the loss in optical texture signatures of axonal fiber bundles in eyes with RNFL defects follows the trajectories of axonal fiber bundles (Fig 1, third column). We demonstrated that ROTA attained a higher specificity and sensitivity for detection of RNFL defects in early glaucoma (i.e., VF MD ≥ -6 dB) than conventional OCT RNFL and ganglion cell–inner plexiform layer (GCIPL) thickness analysis using VF or red-free RNFL photography results as the reference standard.¹³

Measurement of the Area and the Angular Location of RNFL Defects

The area and the angular location of RNFL defects of an individual eye were measured using a custom program developed in MATLAB (MathWorks). The steps are as follows. First, 12 Bruch's membrane opening (BMO) locations from 5 evenly spaced horizontal OCT B-scans and 1 vertical OCT B-scan covering the optic disc were detected manually, and the BMO margin was delineated with ellipse fitting. The BMO center was located as the midpoint of the major and minor axes of the outlined ellipse (Fig 3A). Second, the foveola, detected from the location with the smallest RNFL thickness in the $12 \times 9\text{-mm}^2$ RNFL thickness map, and the BMO center were transposed onto the ROTA map to set the foveola–BMO center axis for annotation of the angle meridians along the BMO margin, with 0° corresponding to temporal meridian, 90° corresponding to the superior meridian, 180° corresponding to the nasal meridian, and 270° corresponding to the inferior meridian (Fig 3B). Third, the area and the angular location (with reference to the BMO margin) of RNFL defects in each hemiretina were generated automatically from the program after the borders of RNFL defect were demarcated using a curve tracing tool developed in MATLAB (Fig 3C). For simplicity, the superior and inferior hemiretinas were divided by the foveola–BMO center axis.

Location-by-Location Structure–Function Mapping

The steps to map the VF stimulus projections of the 24-2 VF test onto the corresponding ROTA map of an eye are as follows. First, the BMO center and the foveola were marked on the ROTA map as described above (Fig 2A). Second, the coordinates of the center of VF blind spot (x, y) expressed in degrees relative to the central fixation (0° , 0°) were exported from the Humphrey Field Analyzer (Fig 2B, left) and transposed onto the BMO center and the foveola of the ROTA map, respectively (Fig 2B, right), to set the scale (pixels per degree) for mapping of the VF stimulus projections. Third, individual VF stimulus projections, 0.43° in size (Goldmann size III) and spaced 6° apart, in the superior hemifield were mapped onto the inferior hemiretina of the ROTA map and vice versa with reference to the mapping scale of an individual eye (Fig 2C). To minimize mapping of VF locations onto the edges of OCT scans, only the central $10 \times 7\text{-mm}^2$ region covering the parapapillary region and the macula were analyzed. A VF stimulus was considered to have projected onto an RNFL defect when at least 50% of the projection area (i.e., 50% of the 0.43° Goldmann size III projection) overlapped with the RNFL defect (Fig S2, available at www.aaojournal.org). The structure–function association was analyzed with multilevel logistic regression analysis (described below).

Statistical Analyses

Statistical analyses were performed with STATA software, version 15.0 (StataCorp). The structure–function association was analyzed using univariable and multivariable multilevel logistic regression models after adjustment of clustering of multiple locations of a single VF and clustering between fellow eyes of a patient to determine (1) whether the size of RNFL defects (in terms of the area or the angular width of RNFL defects along the BMO margin) and the pattern of RNFL defects (in terms of whether the arcuate bundle, papillomacular bundle, or papillofoveal bundle was involved) over a hemiretina would be associated with VF defects in the corresponding hemifield (i.e., ≥ 3 significant [$P < 0.05$] nonedge contiguous locations with at least 1 location with $P < 0.01$) and (2) whether a VF stimulus projected onto an RNFL defect (i.e., with at least 50% of the projection area overlapped with the RNFL defect) would be associated with an abnormal probability value (i.e., $P < 0.05$) in the corresponding location in the VF pattern deviation probability plot. P values < 0.05 were considered statistically significant.

Results

Retinal nerve fiber layer optical texture analysis uncovers the optical texture and trajectories of axonal fiber bundles of the retina in a wide field, revealing RNFL defects over the arcuate bundle (Fig 1A), papillomacular bundle (Fig 1B), and papillofoveal bundle (Fig 1C). The arcuate bundle represented the axonal fiber bundle along the superior and inferior temporal retinal vascular arcades outside the macula (18° , or approximately 5.5 mm; Fig 4A); the papillomacular bundle represented the axonal fiber bundles projected from the macula (Fig 4B), except those projected from the fovea (5° , or approximately 1.5 mm), which were termed the *papillofoveal bundle* in this study (Fig 4C). We further classified papillofoveal bundle into (1) the arcuate papillofoveal bundle, which comprised axonal fiber bundles projected from the temporal fovea arching over the foveola to the optic disc (Fig 4D), and (2) the horizontal papillofoveal bundle, which comprised axonal fiber bundles running largely parallel to the foveola–BMO center axis from the nasal fovea to the optic disc (Fig 4E). Additional examples of RNFL defects involving the arcuate and horizontal papillofoveal bundles are shown in Figure S1.

Patterns of RNFL Defects in Early Glaucoma

Two hundred four eyes of 171 consecutively recruited patients with early glaucoma (i.e., VF MD ≥ -6 dB) were included in the analysis (Table S1, available at www.aaojournal.org). The area of RNFL defects detected by ROTA in an eye varied from 1.0 to 31.7 mm^2 (mean \pm standard deviation (SD), $11.9 \pm 7.0\text{ mm}^2$), corresponding to 1.4% to 45.3% (mean \pm SD, $17.0 \pm 10.0\%$) of the $10 \times 7\text{-mm}^2$ region of analysis. The smallest RNFL defect spanned 0.0° along the BMO margin, whereas the widest RNFL defect extended over 111.4° . The RNFL defect frequency distribution topography (Fig 5A), generated by overlaying the 204 ROTA RNFL defect maps (Fig 3D) with alignment of the BMO center and the foveola of individual eyes, showed that RNFL defects in early glaucoma largely were localized between 50° and 73° along the superotemporal BMO margin, where the superior arcuate bundle converged, and between 296° and 326° along the inferotemporal BMO margin, where the inferior papillomacular bundle converged (Fig 5B). By contrast, axonal fiber bundles converging between 20° and 33° , which corresponded the superior papillomacular and papillofoveal bundle, were least affected in early glaucoma (Fig 5C). Similar

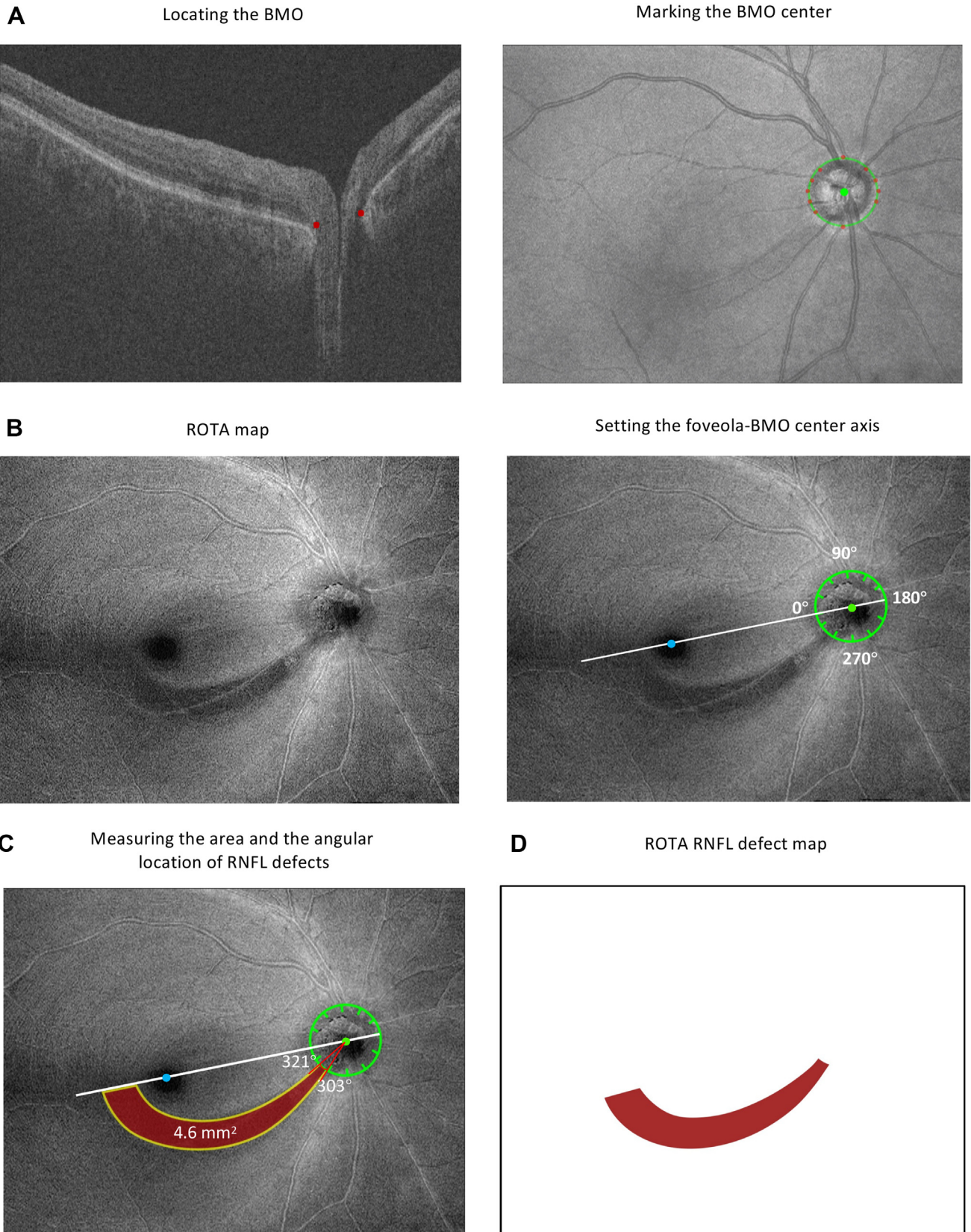


Figure 3. Measurement of the area and the angular location of retinal nerve fiber layer (RNFL) defects. **A**, Locations of Bruch's membrane opening (BMO; red dots, left panel) were identified from 5 evenly spaced horizontal OCT B-scans and 1 vertical OCT B-scan covering the optic disc. The BMO margin was

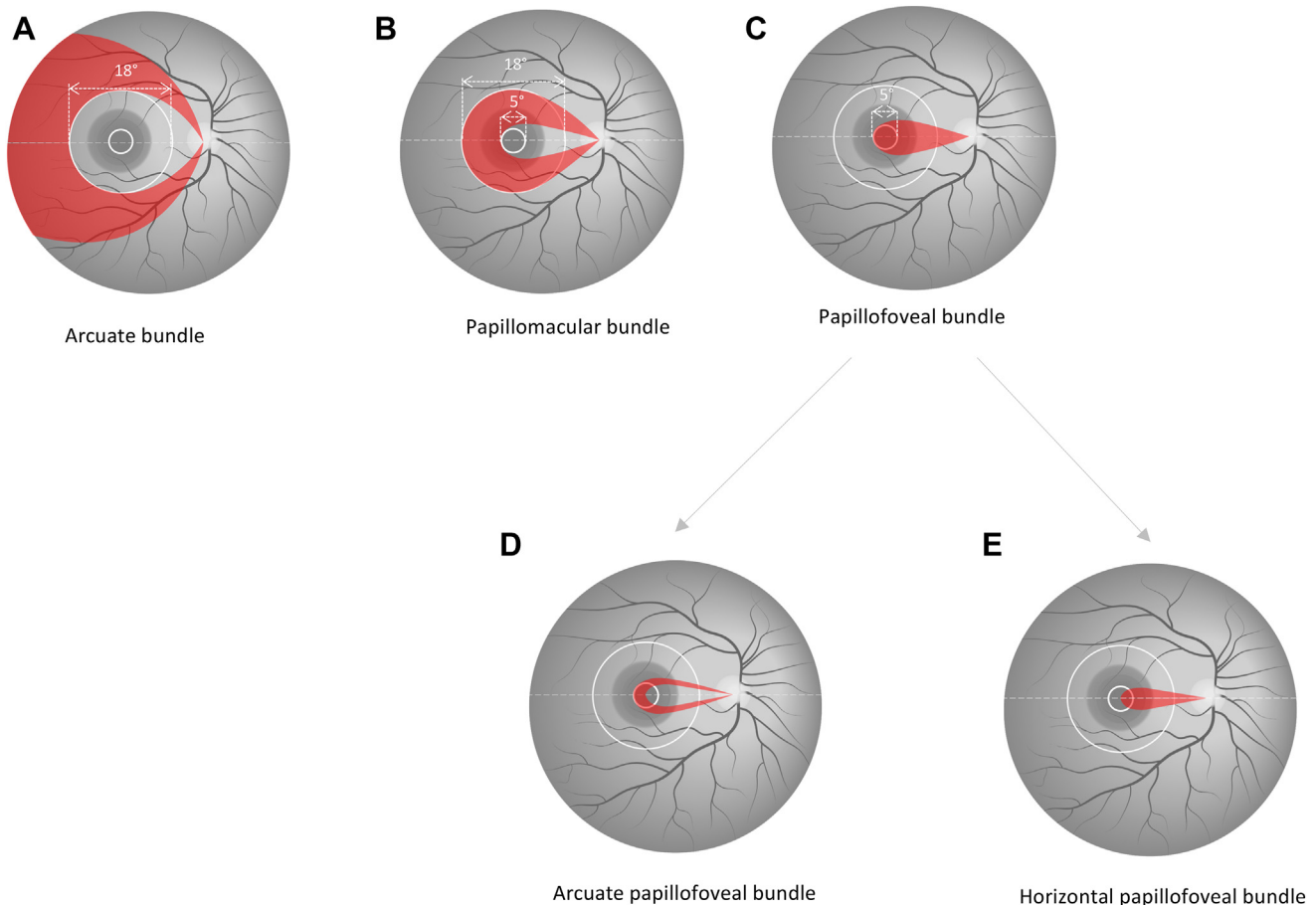


Figure 4. Types of axonal fiber bundles classified by their origins on the retina. **A**, Arcuate bundle arises outside the macula (18°, or approximately 5.5 mm) along the superior and inferior temporal vascular arcades. **B**, Papillomacular bundle comprises axonal fiber bundles projected from the macula, except those projected from the fovea (5°, or approximately 1.5 mm). **C**, Papillofoveal bundle contains axonal fiber bundles projected from the fovea. **D**, **E**, The papillofoveal bundle is classified further into (**D**) the arcuate papillofoveal bundle, which comprises axonal fiber bundles projected from the temporal fovea arching over the foveola to the optic disc, and (**E**) horizontal papillofoveal bundle, which comprises axonal fiber bundles running largely parallel to each other from the nasal fovea to the optic disc.

patterns of RNFL defect frequency distribution were observed for eyes with MD of -6 dB or more and < -3 dB (113 eyes) and for eyes with MD of -3 dB or more (91 eyes; Fig S3, available at www.aaojournal.org).

The patterns of RNFL defects varied widely in early glaucoma; 45.1% of eyes (92 eyes) with early glaucoma showed RNFL defects involving both the superior and inferior hemiretinas (Fig 6, green partitions), 23.0% of eyes (47 eyes) showed superior RNFL defects alone (Fig 6, yellow partitions), and 31.9% of eyes (65 eyes) showed inferior RNFL defects alone (Fig 6, blue partitions). One hundred eighteen eyes (57.8%) showed 2 or more RNFL defects on the retina, among which 92 eyes showed RNFL defects on both hemiretinas and 26 eyes showed 2 or more RNFL defects localized on 1 hemiretina (12 eyes with

superior defects and 14 eyes with inferior defects). The 3 most common patterns of RNFL defects were those involving (1) the inferior arcuate bundle and the inferior papillomacular bundle (20.6% [42 eyes]), (2) the superior arcuate bundle (12.3% [25 eyes]), and (3) the arcuate bundle and the papillomacular bundle over the superior as well as the inferior hemiretina (10.3% [21 eyes]; Fig 6, boldface partitions).

Involvement of Papillomacular Bundle and Papillofoveal Bundle in Early Glaucoma

Of the 204 eyes, 71.6% (146 eyes) showed papillomacular bundle defects; 35.8% of eyes (73 eyes) involved the inferior hemiretina, 15.2% of eyes (31 eyes) involved the superior hemiretina, and

delineated with ellipse fitting (green); the BMO center was marked as the midpoint of the major and minor axes of the outlined ellipse (green dot, right panel). **B**, The foveola (blue dot, right panel), identified from the location with the smallest RNFL thickness in the 12×9 -mm² RNFL thickness map, and the BMO center were transposed onto the corresponding RNFL optical texture analysis (ROTA) map to set the foveola–BMO center axis (white line) for annotation of the angle meridians along the BMO margin, with 0° corresponding to temporal meridian, 90° corresponding to the superior meridian, 180° corresponding to the nasal meridian, and 270° corresponding to the inferior meridian. **C**, Area and the angular location of RNFL defects in each hemiretina, which was separated by the foveola–BMO center axis, were measured after the borders of RNFL defects were demarcated using a curve tracing tool. **D**, The ROTA RNFL defect map was extracted to generate the RNFL defect frequency distribution topography (see Fig 5).

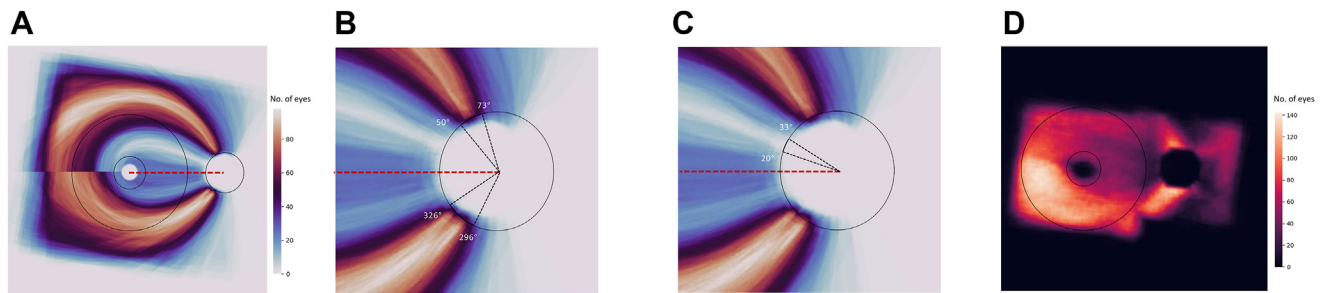


Figure 5. Retinal nerve fiber layer (RNFL) defect frequency distribution topography. **A**, The RNFL defect frequency distribution topography was generated by overlaying the RNFL optical texture analysis (ROTA) RNFL defect maps (Fig 3D) with alignment of the Bruch's membrane opening (BMO) center and foveola from the 204 eyes with early glaucoma. **B**, The RNFL defects largely were localized over the superior arcuate bundle between 50° and 73° along the disc margin and over the inferior papillomacular bundle between 296° and 326°. **C**, The least frequent location where RNFL defects were found was between 20° and 33°, which corresponded to the superior papillomacular and papillofoveal bundle. **D**, Conventional OCT RNFL and ganglion cell–inner plexiform layer (GCIPL) thickness analysis lacks the precision to uncover the trajectories of the axonal fiber bundles; the RNFL thickness probability maps of the parapapillary region and the GCIPL thickness probability maps of the macula from the same OCT scans were overlaid with alignment of the foveola and BMO center to construct the frequency distribution topography. The foveola–BMO center axis, a reference line to define the clockwise meridional locations along the BMO margin, is highlighted in a red dotted line in (A), (B), and (C).

20.6% of eyes (42 eyes) involved both hemiretinas. This result aligns with the findings by Hood⁹ and Hood et al,¹⁰ suggesting the inferotemporal macula to be a vulnerable zone for glaucoma. What remains unclear is whether axonal fiber bundles emanated from the fovea also can be compromised in early glaucoma. Surprisingly, 17.2% of eyes (35 eyes) with early glaucoma showed papillofoveal bundle defects (Fig S4, available at www.aajournal.org); the inferior arcuate papillofoveal bundle was affected most frequently (33 eyes), followed by the inferior horizontal papillofoveal bundle (28 eyes), the superior arcuate papillofoveal bundle (25 eyes), and the superior horizontal papillofoveal bundle (24 eyes). Although the RNFL and GCIPL thickness abnormality frequency distribution topography generated from overlaying the 204 RNFL and GCIPL thickness probability maps derived from the same OCT scans for ROTA also demonstrated RNFL and GCIPL thickness over the inferotemporal macula frequently to be abnormal (Fig 5D), it lacked the precision to reveal the trajectories of the papillofoveal bundle and the papillomacular bundle.

Association between RNFL Defects and VF Defects



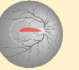


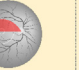
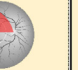



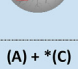
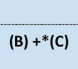
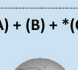

Analysis by Hemifields. Defining VF defects as having 3 or more significant ($P < 0.05$) nonedge contiguous points with at least 1 with a P value of < 0.01 on a hemifield, 21.6% (44 eyes) showed VF defects involving both hemifields, 72.1% (147 eyes) showed VF defects restricted to 1 hemifield (66 eyes showed inferior VF defects, and 81 eyes showed superior VF defects), and 6.4% (13 eyes) showed no VF defects. Among the 408 hemiretinas of the 204 eyes, 296 hemiretinas showed RNFL defects, among which 27.7% (82/296) showed an intact VF in the corresponding hemifield. The RNFL defects with a greater defect area (odds ratio, 1.15 per 1 mm^2 more; 95% confidence interval [CI], 1.06–1.24 per 1 mm^2 more) or with a greater angular width at the BMO margin (odds ratio, 1.03 per 1° more; 95% CI, 1.01–1.05 per 1° more) on a hemiretina were more likely to be associated with VF defects in the corresponding hemifield. Eyes with RNFL defects involving the arcuate bundle on a hemiretina showed a higher risk of VF defects in the corresponding hemifield than those without the involvement of the arcuate bundle, with (Table S2, available at www.aajournal.org) or without (Table 1) adjustment of the area or the angular width of RNFL defects. However, eyes with

RNFL defects involving the papillomacular bundle or the papillofoveal bundle in a hemiretina were not associated with VF defects in the corresponding hemifield (Table 1).

Analysis by Individual VF Test Locations. Because only the central 4 VF locations correspond to the macula in the 24-2 test (all the other VF stimulus projections reside beyond the central 18° ; Fig S5, available at www.aajournal.org), we examined further the association between papillomacular and papillofoveal bundle defects and VF sensitivity abnormality over the 4 central VF locations. Among the 816 central VF test locations (4×204) of the 204 eyes with early glaucoma, 103 locations (12.6%) and 63 locations (7.7%) showed an abnormal pattern deviation probability value at $P < 0.05$ and $P < 0.005$, respectively. Visual field sensitivity of a stimulus projected onto an RNFL defect (with at least 50% of the projection area overlapped with the RNFL defect) showed a 12.5-fold (95% CI, 7.0–22.5) and 16.8-fold (95% CI, 8.5–33.1) increase in odds of being abnormal at $P < 0.05$ and $P < 0.005$, respectively, in the VF pattern deviation probability plot, compared with that projected onto a location with an intact papillomacular or papillofoveal bundle, after adjustment of clustering of multiple VF locations within an eye and clustering between fellow eyes within a patient (Table 2). Similar findings were observed when all VF stimulus projections within the $10 \times 7\text{-mm}^2$ region of analysis were taken into consideration (Table 2).

Discussion

Although early involvement of the macula in glaucoma has been described,^{9–12} our understanding of the pattern and the extent of the axonal fiber bundle damage on the macula remains imprecise (Fig 5D), which is connected to the lack of a robust and reliable clinical tool to examine axonal fiber bundle loss. The novelty of this study stems from the application of ROTA, a more precise approach to unveil the optical texture and trajectories of axonal fiber bundles than red-free photography and conventional OCT analysis,¹³ to characterize papillofoveal bundle defects and papillomacular bundle defects in addition to other patterns of axonal fiber bundle loss in early glaucoma. Contrary to the conventional notion that glaucomatous optic nerve

		Superior Hemiretina (yellow)							Total: 47 eyes (23.0%)
		(A) Arcuate bundle	(B) Papillomacular bundle	* (C) Papillofoveal bundle	(A) + (B)	(A) + * (C)	(B) + * (C)	(A) + (B) + * (C)	
									
		25 (12.3%)	1 (0.5%)		20 (9.8%)	1 (0.5%)			
Inferior Hemiretina (blue)	(A) Arcuate bundle		10 (4.9%)	16 (7.8%)	1 (0.5%)		2 (1.0%)		
	(B) Papillomacular bundle		9 (4.4%)	4 (2.0%)		7 (3.4%)			
	* (C) Papillofoveal bundle				1 (0.5%)		2 (1.0%)		4 (2.0%)
	(A) + (B)		42 (20.6%)	10 (4.9%)	1 (0.5%)		21 (10.3%)		
	(A) + * (C)					2 (1.0%)	1 (0.5%)	1 (0.5%)	2 (1.5%)
	(B) + * (C)			1 (0.5%)			2 (1.0%)		5 (2.5%)
	(A) + (B) + * (C)		4 (2.0%)			2 (1.0%)	1 (0.5%)	2 (1.0%)	4 (2.0%)
Total: 65 eyes (31.9%)							Total: 92 eyes (45.1%)		

*Papillofoveal bundle includes arcuate papillofoveal bundle (Fig.4D) or horizontal papillofoveal bundle (Fig.4E).

Figure 6. Patterns of retinal nerve fiber layer (RNFL) defects in early glaucoma. The frequency distribution matrix of RNFL defects classified by the involvement of the arcuate bundle, papillomacular bundle, papillofoveal bundle, or any combination of the above over the superior hemiretina (yellow), the inferior hemiretina (blue), and both hemiretinas (green) in 204 eyes with early glaucoma. The numbers indicated in the matrix denote the number of eyes and the corresponding proportion. The first row and the first column of the matrix depict the anatomic region of arcuate bundle, papillomacular bundle, and papillofoveal bundle; an eye with RNFL defects over a particular region may have complete or partial involvement of that region. The 3 most common patterns of RNFL defects appear in boldface.

Table 1. Univariable Multilevel Logistic Regression Analysis of the Association between the Extent and the Type of RNFL Defects on a Hemiretina and the Detection of Visual Field Defects (≥ 3 Contiguous Locations with Abnormal Visual Field Sensitivity in the Pattern Deviation Probability Plot) in the Corresponding Hemifield

	Odds Ratio (95% Confidence Interval)	P Value
RNFL defect area (per 1 mm ² more)*	1.15 (1.06–1.24)	<0.001
RNFL defect angular width (per 1° more)*	1.03 (1.01–1.05)	0.002
Arcuate bundle defect (1 = presence; 0 = absence)	8.03 (3.22–20.0)	<0.001
Papillomacular bundle defect (1 = presence; 0 = absence)	1.16 (0.69–1.96)	0.575
Papillofoveal bundle defect (1 = presence; 0 = absence)	0.61 (0.33–1.11)	0.103

RNFL = retinal nerve fiber layer.

*Retinal nerve fiber layer defect area and RNFL defect angular width include the measurements of all RNFL defects detected by RNFL optical texture analysis in a hemiretina.

damage in the early stages is characterized by focal loss of the RNFL, which is confined to a hemiretina (which is the basis of the glaucoma hemifield test for detection of VF defects in glaucoma) and spares the fovea, our study showed that multiple RNFL defects over both hemiretinas and involvement of the papillofoveal bundle and papillomacular bundle were common in early glaucoma. Examining 204 eyes with early glaucoma with VF MD of -6 dB or more from 171 consecutively enrolled patients, 45.1% of eyes (92 eyes) showed RNFL defects on both hemiretinas, which contrasts to the smaller proportion of eyes with VF defects on both hemifields (21.6% [44 eyes]; $P < 0.001$). Strikingly, 71.6% of eyes (146 eyes) harbored papillomacular bundle defects, and 17.2% of eyes (35 eyes) harbored papillofoveal bundle defects, and they were associated with central VF sensitivity loss at the corresponding test locations in the 24-2 test (Table 2), although using the conventional criteria to detect VF defects would miss such abnormalities (Table 1). Our data suggest that ROTA plays an important role in (1) unfolding the diversity of RNFL defects, (2) uncovering the involvement of the papillomacular and papillofoveal bundles, and (3) unraveling the structure–function discordance in early glaucoma.

Unfolding the Diversity of RNFL Defects

A distinct advantage of ROTA to evaluate RNFL defects stems from its ability to discern the trajectorial details of axonal fiber bundles within and beyond the macula. Uncovering the papillomacular bundle, not only the papillofoveal bundle, is difficult in clinical practice. The papillomacular bundle originally was described in an autopsy study by Uhthoff²³ in 1866, when he named the degenerated optic nerve fibers associated with cecentral scotoma in vitamin B₁₂ deficiency-related optic neuropathy as *papillomakuläre opticusfaser*. Although the papillofoveal bundle has been described in a histologic study in nonhuman primates,²⁴ it has yet to be characterized in human eyes. Clinical assessment of axonal fiber bundles emanating from the fovea is difficult because the RNFL is thin and the corresponding scattering is weak at the parafoveal region. Although the boundaries of arcuate bundle, papillomacular bundle, and papillofoveal bundle are indistinct, it is feasible to differentiate these entities by following their trajectories in ROTA. Such discrimination enables the dissection of the diversity of the location of RNFL defects on the retina (Fig 6). Although the pattern of RNFL defects is diverse in early glaucoma, in this

Table 2. Univariable Multilevel Logistic Regression Analysis of the Association between Retinal Nerve Fiber Layer Defects on a Hemiretina and Abnormal VF Sensitivities at the Corresponding Locations (Fig 2)

Abnormal VF Sensitivity	Odds Ratio (95% Confidence Interval)	P Value
Central 4 VF stimulus projections (over the macula)		
$P < 0.05$	12.49 (6.95–22.46)	<0.001
$P < 0.02$	14.43 (7.88–26.41)	<0.001
$P < 0.01$	17.78 (9.07–34.88)	<0.001
$P < 0.005$	16.77 (8.49–33.13)	<0.001
All VF stimulus projections (over the 10 × 7-mm ² ROTA map)		
$P < 0.05$	6.81 (5.65–8.21)	<0.001
$P < 0.02$	7.91 (6.43–9.74)	<0.001
$P < 0.01$	8.22 (6.60–10.23)	<0.001
$P < 0.005$	8.49 (6.63–10.86)	<0.001

ROTA = retinal nerve fiber layer optical texture analysis; VF = visual field.

The odds ratios of a VF location being abnormal at $P < 0.05$, $P < 0.02$, $P < 0.01$, or $P < 0.005$ in the pattern deviation probability plot when the VF stimulus was projected onto an retinal nerve fiber layer defect (i.e., with at least 50% of the projection area overlapped with the retinal nerve fiber layer defect) are shown.

study, they were highly localized at the BMO margin (Fig 5B), spanning about 23° in the superior hemiretina (between 50° and 73° where the superior arcuate bundle converged) and about 30° in the inferior hemiretina (between 296° and 326° where the inferior papillomacular bundle converged). The relatively focal confinement of RNFL defects at the BMO margin corroborates the existence of biomechanical weak points at the lamina cribrosa.^{25,26}

Uncovering the Involvement of the Papillomacular Bundle and Papillofoveal Bundle

Glaucoma has been depicted as an optic neuropathy impairing the peripheral vision but sparing the central vision in its early stages. However, ROTA showed that only 25.0% of eyes with early glaucoma exhibit isolated arcuate bundle defects (12.3% harbored a superior arcuate defect, 4.9% harbored an inferior arcuate defect, and 7.8% harbored superior and inferior arcuate defects; Fig 6), whereas the remaining 75.0% harbored varying degrees of papillomacular bundle or papillofoveal bundle loss or both. The high proportion of eyes with inferior papillomacular bundle defects is reminiscent of and consistent with the inferior vulnerability zone in the RNFL thickness and GCIPL thickness probability maps described by Hood⁹ and Hood et al.¹⁰ Adding to their finding, our study highlights the unanticipated involvement of the papillofoveal bundle, which would not otherwise be discernible with conventional OCT RNFL and GCIPL thickness analysis (Fig 5D). Preserving the papillofoveal and papillomacular bundles is essential in the management of patients with glaucoma; a more intensive monitoring and treatment regimen would be indicated in patients with papillomacular bundle defects, and more so with papillofoveal bundle defects, because of a higher risk of central vision loss and development of visual disability.

Unraveling the Structure–Function Discordance in Early Glaucoma

Notably, only eyes with arcuate bundle defects, but not those with papillofoveal and papillomacular bundle defects, were associated with VF defects in the corresponding hemifield in the 24-2 VF test (Table 1). The structure–function discordance is attributed to the fact that only 4 VF locations of the 24-2 VF test correspond to the macula (18°; Fig S5); requiring 3 contiguous abnormal VF locations on a hemifield in the VF pattern deviation probability plot to detect a VF defect would miss VF sensitivity loss consequential to papillomacular or papillofoveal bundle defects or both on a hemiretina (Fig 1B, C; Fig S1A). Nevertheless, VF defects associated with papillomacular or papillofoveal bundle defects could be detected in the 24-2 test when concomitant involvement of the arcuate bundle was present (Fig S1B; the papillofoveal bundle defect and the papillomacular bundle and arcuate bundle defect over the inferior hemiretina were associated with the superior paracentral and nasal VF defects). The structure–function association analysis by

hemifields supports the validity of ROTA in discriminating arcuate bundle defects versus papillomacular and papillofoveal bundle defects. With location-by-location structure–function mapping (Fig 2), VF sensitivity abnormalities associated with papillomacular and papillofoveal bundle defects were evident at the corresponding locations (Table 2). Our results underscore the importance of applying VF tests with a higher sampling density over the central 18°, like the 10-2 test and the 24-2C test,^{27–29} to detect VF loss associated with papillomacular and papillofoveal bundle defects (the lack of the 10-2 test or 24-2C test is a study limitation). On a similar note, our finding cautions against the labeling of preperimetric glaucoma without considering the spatial correspondence between VF stimulus projections and RNFL defects.

Strengths and Limitations of ROTA

Although the trajectories of axonal fiber bundles sometimes can be visualized in red-free RNFL photographs and en face OCT reflectance projection, ROTA is more robust and reliable in revealing the trajectories of axonal fiber bundles over a wide field of the retina; RNFL defects missed by red-free RNFL photography and en face OCT can be uncovered by ROTA.¹³ Although the detection of RNFL defects with ROTA, like red-free photography, is not accomplished using a normative distribution, ROTA showed high interobserver agreement ($\kappa = 0.95–0.96$), test–retest agreement ($\kappa = 0.97$), high sensitivity (97.3%–98.4%), and high specificity (94.3%–96.1%) to detect RNFL defects in early glaucoma, which outperformed conventional OCT analysis with RNFL and GCIPL abnormalities defined with reference to the normative distribution of RNFL and GCIPL thicknesses.¹³ The fact that the borders of RNFL defects, which can be delineated distinctively in ROTA because they confine to the trajectories of axonal fiber bundles, has facilitated unambiguous recognition of RNFL defects which otherwise would be obscured in red-free photography and conventional OCT analysis. Whereas location-by-location mapping for structure–function association analysis is possible with ROTA (Fig 2), eccentricity mismatch (i.e., a VF stimulus projected onto an area of RNFL defect with a relatively well-preserved retinal ganglion cell density may show normal VF sensitivity) could weaken the structure–function association. Nevertheless, the relatively high odds ratios observed in the location-by-location analysis (Table 2) suggest that most test locations examined in the study did not have notable eccentricity mismatch.

Conclusions

Through unveiling the diversity of RNFL defects, informing the involvement of the papillofoveal and papillomacular bundles, and bridging the disconnect in structure and function, ROTA has the potential to reset the paradigm in the diagnostic evaluation and management of patients with glaucoma.

Footnotes and Disclosures

Originally received: November 14, 2021.

Final revision: March 31, 2022.

Accepted: April 18, 2022.

Available online: ■■■■. Manuscript no. OPHTHA-D-21-02244.

¹ Department of Ophthalmology, LKS Faculty of Medicine, The University of Hong Kong, Hong Kong, People's Republic of China.

² Department of Ophthalmology, Queen Mary Hospital, Pok Fu Lam, Hong Kong, People's Republic of China.

³ Hong Kong Eye Hospital, Kowloon City, Hong Kong, People's Republic of China.

Disclosure(s):

All authors have completed and submitted the ICMJE disclosures form.

The author(s) have made the following disclosure(s): C.K.S.L.: Financial and Nonfinancial support and License fees – Carl Zeiss Meditec, Heidelberg Engineering, Topcon; Advisory board – Santen; Lecturer – Topcon, Santen, Carl Zeiss Meditec; Patent (US patent 62/571,559) – Retinal nerve fiber layer optical texture analysis; Founder - AIROTA Diagnostics Limited A.K.N.L.: Patent (US patent 62/571,559) – Retinal nerve fiber layer optical texture analysis; Co-Founder – AIROTA Diagnostics Limited

Supported by the Hong Kong Research Grants Council General Research Fund, Hong Kong, China (grant nos.: 14101518, 14101117, 14100916, and 14101215). The funder had no role in the initiation or design of the study, collection of samples, analysis, interpretation of data, writing of the paper, or the submission for publication. The study and researchers are independent of the funder.

The full study protocol and study data can be obtained upon request from the corresponding author.

HUMAN SUBJECTS: Human subjects were included in this study. The study adhered to the Declaration of Helsinki and was approved by the Hong Kong Hospital Authority research ethics committees with written informed consent obtained.

No animal subjects were included in this study.

Author Contributions:

Conception and design: Leung

Analysis and interpretation: Leung, Guo, Lam

Data collection: Leung, Guo, Lam

Obtained funding: Leung

Overall responsibility: Leung, Guo, Lam

Abbreviations and Acronyms:

BMO = Bruch's membrane opening; **CI** = confidence interval; **GCIPL** = ganglion cell–inner plexiform layer; **MD** = mean deviation; **RNFL** = retinal nerve fiber layer; **ROTA** = retinal nerve fiber layer optical texture analysis; **SD** = standard deviation; **VF** = visual field.

Keywords:

Glaucoma, OCT, Retinal nerve fiber layer, Retinal nerve fiber layer optical texture analysis, ROTA.

Correspondence:

Christopher K. S. Leung, MD, MBChB, Department of Ophthalmology, LKS Faculty of Medicine, The University of Hong Kong, Hong Kong, People's Republic of China. E-mail: cleung21@hku.hk.

References

- Vogt A. Herstellung eines gelbblauen Lichtfiltrates, in welchem die Macula centralis in vivo in gelber Färbung erscheint, die Nervenfasern der Netzhaut und andere feine Einzelheiten derselben sichtbar werden, und der Grad der Gelbfärbung der Linse ophthalmoskopisch nachweisbar ist. *Gräfes Archiv Ophthalmol.* 1913;84:293–311.
- Hoyt WF, Frisén L, Newman NM. Fundoscopy of nerve fiber layer defects in glaucoma. *Invest Ophthalmol.* 1973;12:814–829.
- Huang D, Swanson EA, Lin CP, et al. Optical coherence tomography. *Science.* 1991;254:1178–1181.
- Leung CK, Lam S, Weinreb RN, et al. Retinal nerve fiber layer imaging with spectral-domain optical coherence tomography: analysis of the retinal nerve fiber layer map for glaucoma detection. *Ophthalmology.* 2010;117:1684–1691.
- Leung CK. Diagnosing glaucoma progression with optical coherence tomography. *Curr Opin Ophthalmol.* 2014;25:104–111.
- Wu K, Lin C, Lam AK, et al. Wide-field trend-based progression analysis of combined retinal nerve fiber layer and ganglion cell inner plexiform layer thickness: a new paradigm to improve glaucoma progression detection. *Ophthalmology.* 2020;127:1322–1330.
- Oddone F, Lucenteforte E, Michelessi M, et al. Macular versus retinal nerve fiber layer parameters for diagnosing manifest glaucoma: a systematic review of diagnostic accuracy studies. *Ophthalmology.* 2016;123:939–949.
- Biswas S, Lin C, Leung CK. Evaluation of a myopic normative database for analysis of 530 retinal nerve fiber layer thickness. *JAMA Ophthalmol.* 2016;134:1032–1039.
- Hood DC. Improving our understanding, and detection, of glaucomatous damage: an approach based upon optical coherence tomography (OCT). *Prog Retin Eye Res.* 2017;57:46–75.
- Hood DC, Raza AS, de Moraes CG, et al. Glaucomatous damage of the macula. *Prog Retin Eye Res.* 2013;32:1–21.
- Garg A, Hood DC, Pensec N, et al. Macular damage, as determined by structure-function staging, is associated with worse vision-related quality of life in early glaucoma. *Am J Ophthalmol.* 2018;194:88–94.
- Hirji SH, Liebmann JM, Hood DC, et al. Macular damage in glaucoma is associated with deficits in facial recognition. *Am J Ophthalmol.* 2020;217:1–9.
- Leung CK, Lam AKN, Weinreb RN, et al. Diagnostic assessment of glaucoma and non-glaucomatous optic neuropathy via retinal nerve fiber layer optical texture analysis. *Nat Biomed Eng.* 2022;6(5):593–604. <https://doi.org/10.1038/s41551-021-00813-x>. Online ahead of print.
- Sommer A, Quigley HA, Robin AL, et al. Evaluation of nerve fiber layer assessment. *Arch Ophthalmol.* 1984;102:1766–1771.
- Centre for Clinical Research and Biostatistics—Clinical Trials Registry. Hong Kong (partner of Chinese Clinical Trial Registry, Sichuan, China): The Chinese University of Hong Kong. Identifier CUHK_CCRB00439: progressive lamina cribrosa deformation—a biomarker for fast progressors in glaucoma? November 24, 2014. Available at: <https://www2.ccrb.cuhk.edu.hk/registry/public/278>. Accessed November 1, 2021.
- Centre for Clinical Research and Biostatistics—Clinical Trials Registry. Hong Kong (partner of Chinese Clinical Trial Registry, Sichuan, China): The Chinese University of Hong Kong.

- Identifier CUHK_CCRB00591: measurement of the rates of retinal nerve fiber layer thinning to guide management of glaucoma patients. March 9, 2014. Available at: <https://www2.crb.cuhk.edu.hk/registry/public/457>. Accessed November 1, 2021.
17. Australian New Zealand Clinical Trials Registry. Sydney (NSW): NHMRC Clinical Trials Centre, University of Sydney (Australia); 2005. Identifier ACTRN12618000453280: progressive retinal nerve fiber layer (RNFL) thinning as a biomarker to guide intraocular pressure (IOP) lowering treatment in ocular hypertensives (OHT). March 28, 2018. Available at: <https://www.anzctr.org.au/Trial/Registration/TrialReview.aspx?id=373418>. Accessed November 1, 2021.
 18. Weinreb RN, Leung CK, Crowston JG, et al. Primary open-angle glaucoma. *Nat Rev Dis Primers*. 2016;2:16067.
 19. Neelam K, Cheung CM, Ohno-Matsui K, et al. Choroidal neovascularization in pathological myopia. *Prog Retin Eye Res*. 2012;31:495–525.
 20. Anderson DR. *Automated Static Perimetry*. 123. St. Louis: Mosby Year Book; 1992.
 21. Pons ME, Ishikawa H, Gürses-Ozden R, et al. Assessment of retinal nerve fiber layer internal reflectivity in eyes with and without glaucoma using optical coherence tomography. *Arch Ophthalmol*. 2000;118:1044–1047.
 22. Vermeer KA, van der Schoot J, Lemij HG, de Boer JF. RPE-normalized RNFL attenuation coefficient maps derived from volumetric OCT imaging for glaucoma assessment. *Invest Ophthalmol Vis Sci*. 2012;53:6102–6108.
 23. Uhthoff W. Untersuchungen über den Einfluss des chronischen Alkoholismus auf das menschliche Sehorgan. *Albrecht von Graefes Archiv für Ophthalmologie*. 1886;32:154–188.
 24. Hiraoka M, Inoue K, Kawano H, Takada M. Localization of papillofoveal bundles in primates. *Anat Rec (Hoboken)*. 2012;295:347–354.
 25. Downs JC, Girkin CA. Lamina cribrosa in glaucoma. *Curr Opin Ophthalmol*. 2017;28:113–119.
 26. Andrade JCF, Kanadani FN, Furlanetto RL, et al. Elucidation of the role of the lamina cribrosa in glaucoma using optical coherence tomography. *Surv Ophthalmol*. 2022;67(1):197–216.
 27. De Moraes CG, Hood DC, Thenappan A, et al. 24-2 Visual fields miss central defects shown on 10-2 tests in glaucoma suspects, ocular hypertensives, and early glaucoma. *Ophthalmology*. 2017;124:1449–1456.
 28. Grillo LM, Wang DL, Ramachandran R, et al. The 24-2 visual field test misses central macular damage confirmed by the 10-2 visual field test and optical coherence tomography. *Transl Vis Sci Technol*. 2016;5:15.
 29. Phu J, Kalloniatis M. Ability of 24-2C and 24-2 grids to identify central visual field defects and structure-function concordance in glaucoma and suspects. *Am J Ophthalmol*. 2020;219:317–331.